Infrared spectroscopy of cataclysmic variables – III. Dwarf novae below the period gap and nova-like variables

V. S. Dhillon,[1]★ S. P. Littlefair,[1] S. B. Howell,[2] D. R. Ciardi,[3] M. K. Harrop-Allin[4] and T. R. Marsh[5]

[1]*Department of Physics and Astronomy, University of Sheffield, Sheffield S3 7RH*
[2]*Astrophysics Group, Planetary Science Institute, 620 North 6th Ave, Tuscon, AZ 85705, USA*
[3]*Department of Astronomy, 211 Bryant Space Sciences Building, University of Florida, Gainesville, FL 32611, USA*
[4]*Mullard Space Science Laboratory, University College London, Holmbury St Mary, Dorking, Surrey RH5 6NT*
[5]*Department of Physics and Astronomy, University of Southampton, Highfield, Southampton SO17 1BJ*

ABSTRACT

We present K-band spectra of the short-period dwarf novae YZ Cnc, LY Hya, BK Lyn, T Leo, SW UMa and WZ Sge, the nova-like variables DW UMa, V1315 Aql, RW Tri, VY Scl, UU Aqr and GP Com, and a series of field dwarf stars with spectral types ranging from K2 to M6.

The spectra of the dwarf novae are dominated by emission lines of H I and He I. The large velocity and equivalent widths of these lines, in conjunction with the fact that the lines are double-peaked in the highest inclination systems, indicate an accretion disc origin. In the case of YZ Cnc and T Leo, for which we obtained time-resolved data covering a complete orbital cycle, the emission lines show modulations in their equivalent widths that are most probably associated with the bright spot (the region where the gas stream collides with the accretion disc). There are no clear detections of the secondary star in any of the dwarf novae below the period gap, yielding upper limits of 10–30 per cent for the contribution of the secondary star to the observed K-band flux. In conjunction with the K-band magnitudes of the dwarf novae, we use the derived secondary star contributions to calculate lower limits to the distances to these systems.

The spectra of the nova-like variables are dominated by broad, single-peaked emission lines of H I and He I – even the eclipsing systems we observed do not show the double-peaked profiles predicted by standard accretion disc theory. With the exception of RW Tri, which exhibits Na I, Ca I and ^{12}CO absorption features consistent with a M0V secondary contributing 65 per cent of the observed K-band flux, we find no evidence for the secondary star in any of the nova-like variables. The implications of this result are discussed.

Key words: accretion, accretion discs – binaries: close – novae, cataclysmic variables – infrared: stars.

1 INTRODUCTION

Cataclysmic variables (CVs) are interacting binary systems in which a white dwarf primary accretes material from a red dwarf secondary (see Warner 1995 for a review). The infrared (IR) is a relatively unexplored part of the spectrum as far as CVs are concerned (see Dhillon 1998 for a review). This is surprising given the fact that the $1-2.5\,\mu m$ wavelength range happens to be where the spectrum of the G–M dwarf secondary star in CVs is expected to peak,[1] and where low-harmonic, cyclotron emission from the weaker field magnetic CVs and emission from the cool, outer

regions of the accretion disc in non-magnetic CVs would be expected to fall. For the above reasons, we embarked on a spectral survey of CVs in the IR, the results of which have been published in Dhillon & Marsh (1995, hereafter Paper I – dwarf novae above the period gap) and Dhillon et al. (1997, hereafter Paper II – intermediate polars).

---

[1] The spectral type of the secondary star in a CV can be determined from its orbital period, P, using the relationships $26.5 - 0.7P$ (for $P < 4\,h$) and $33.2 - 2.5P$ (for $P > 4\,h$), where G0 = 0, K0 = 10 and M0 = 20 (Smith & Dhillon 1998). The wavelength, λ_{max}, of the peak flux, f_ν, for a star of effective temperature T_{eff} can be approximated by $\lambda_{max} = 5100/T_{eff}\,\mu m$. With T_{eff} ranging from $\sim 6000-2000\,K$ for the G–M dwarf secondary stars in CVs, λ_{max} ranges from $\sim 1-2.5\,\mu m$.

★ E-mail: vik.dhillon@sheffield.ac.uk

© 2000 RAS

Two of the types of CV that were not surveyed in Papers I and II were the dwarf novae below the period gap and the nova-like variables. These represent the two classes of CV in which the secondary star has proved to be hardest to detect in optical spectra (e.g. Friend et al. 1988; Smith et al. 1997). In fact, table 1 of Smith & Dhillon (1998) shows that the secondary star has been directly observed in only four dwarf novae below the period gap and four nova-like variables, compared to a total of 55 detections in all classes of CV. In the case of dwarf novae below the period gap, the paucity of secondary star detections is probably caused by the fact that the secondary star is of a very late type and hence faint. In the case of the nova-like variables, the lack of secondary star detections is probably the result of the very bright discs drowning out the light from the companion. If we are to learn anything about the secondary stars in these systems, and hence how these types of CV evolve, some means of detecting the secondary star must be found. Given that light from the disc should be relatively weak in the IR, and that the secondary star should peak in the IR, we decided to perform an IR spectral survey of dwarf novae below the period gap and nova-like variables in order to detect their elusive secondary stars. The results of this survey are presented in this third and final paper in the series.

2 OBSERVATIONS

The data presented in this paper were obtained between 1993 February 8 and 1997 May 28 with the 1–5 µm Cooled Grating Spectrometer 4 (CGS4) on the United Kingdom 3.8-m Infrared Telescope (UKIRT) on Mauna Kea, Hawaii. With the exception of GP Com, which was observed with the instrumental configuration described by Dhillon et al. (1997), all of the spectra presented in this paper were obtained with the 256×256 pixel InSb array, the 75 line mm^{-1} grating in first order and the 150-mm camera, giving a wavelength range of approximately 0.6 µm at a resolution of $350 \, km \, s^{-1}$. Optimum spectral sampling and bad pixel removal were obtained by mechanically shifting the array over 2 pixels in the dispersion direction in steps of 0.5 pixel. We employed the non-destructive readout mode of the detector in order to reduce the readout noise. The slit width was 1.2 arcsec (projecting to 1 pixel on the detector) and the slit was oriented at the parallactic angle. The seeing disc was usually equal to or slightly larger in size than the slit width, except on the night of 1997 May 28, when we employed the new tip-tilt secondary mirror to produce subarcsec images. The observations were all obtained in photometric conditions, apart from the night of 1995 October 21 which

Table 1. Journal of observations. The classifications and orbital periods of the CVs have been taken from the catalogue of Ritter & Kolb (1998). The spectral types of the late-type dwarfs have been taken from the catalogue of Kirkpatrick, Henry & McCarthy (1991), unless otherwise noted. Note that the classification of BK Lyn as the first nova-like variable below the period gap (Dobrzycka & Howell 1992) has been questioned by Ringwald et al. (1996), who speculate that the object may instead be a dwarf nova with rare outbursts akin to those observed in objects like WZ Sge. For the purposes of this paper, we have grouped BK Lyn with the dwarf novae below the period gap.

Object	Class	Period (h)	Date	UTC start	UTC end	Exposure time (s)
Cataclysmic variables
RW Tri	NL UX	5.57	21/10/95	08:30	09:05	1700
VY Scl	NL VY	3.99	21/10/95	07:37	08:18	1900
UU Aqr	NL UX	3.93	21/10/95	09:16	09:32	800
V1315 Aql	NL UX SW	3.35	08/09/95	07:54	08:05	480
DW UMa	NL UX SW	3.28	03/02/97	11:14	11:53	1920
BK Lyn	NL SH?	1.80	06/02/96	10:18	11:14	2880
GP Com	NL AC	0.78	08/02/93	15:39	16:10	1440
YZ Cnc	DN SU	2.08	05/02/96	07:20	11:34	12000
LY Hya	DN	1.80	05/02/96	13:14	15:32	6720
T Leo	DN SU	1.41	06/02/96	13:22	15:25	5760
SW UMa	DN SU DQ?	1.36	06/02/96	07:17	10:11	8160
WZ Sge	DN SU WZ CP	1.36	28/05/97	11:49	14:39	8640

Object	Spectral type	Date	UTC start	UTC end	Exposure time (s)
Late-type dwarfs
Gl764.1A	K2V[a]	20/10/95	07:26	07:35	192
Gl775	K5V	20/10/95	06:20	06:27	96
Gl764.1B	K7V	20/10/95	05:43	05:52	240
Gl154	M0V[b]	21/10/95	09:39	09:48	192
Gl763	M0V	20/10/95	06:00	06:08	144
Gl229	M1V	06/02/96	05:00	05:08	72
Gl806	M2V	20/10/95	07:12	07:21	192
Gl436	M3V	05/02/96	11:56	12:06	192
Gl748AB	M3.5V	28/05/97	11:17	11:26	576
Gl402	M4V	05/02/96	11:41	11:46	120
Gl866AB	M5V	21/10/95	05:25	05:33	192
Gl473AB	M5.5V[c]	06/02/96	15:44	16:02	288
Gl65AB	M6V	05/02/96	05:14	05:22	192

[a] (Gliese 1969).
[b] Hawley, Gizis & Reid (1996).
[c] Henry, Kirkpatrick & Simons (1994).

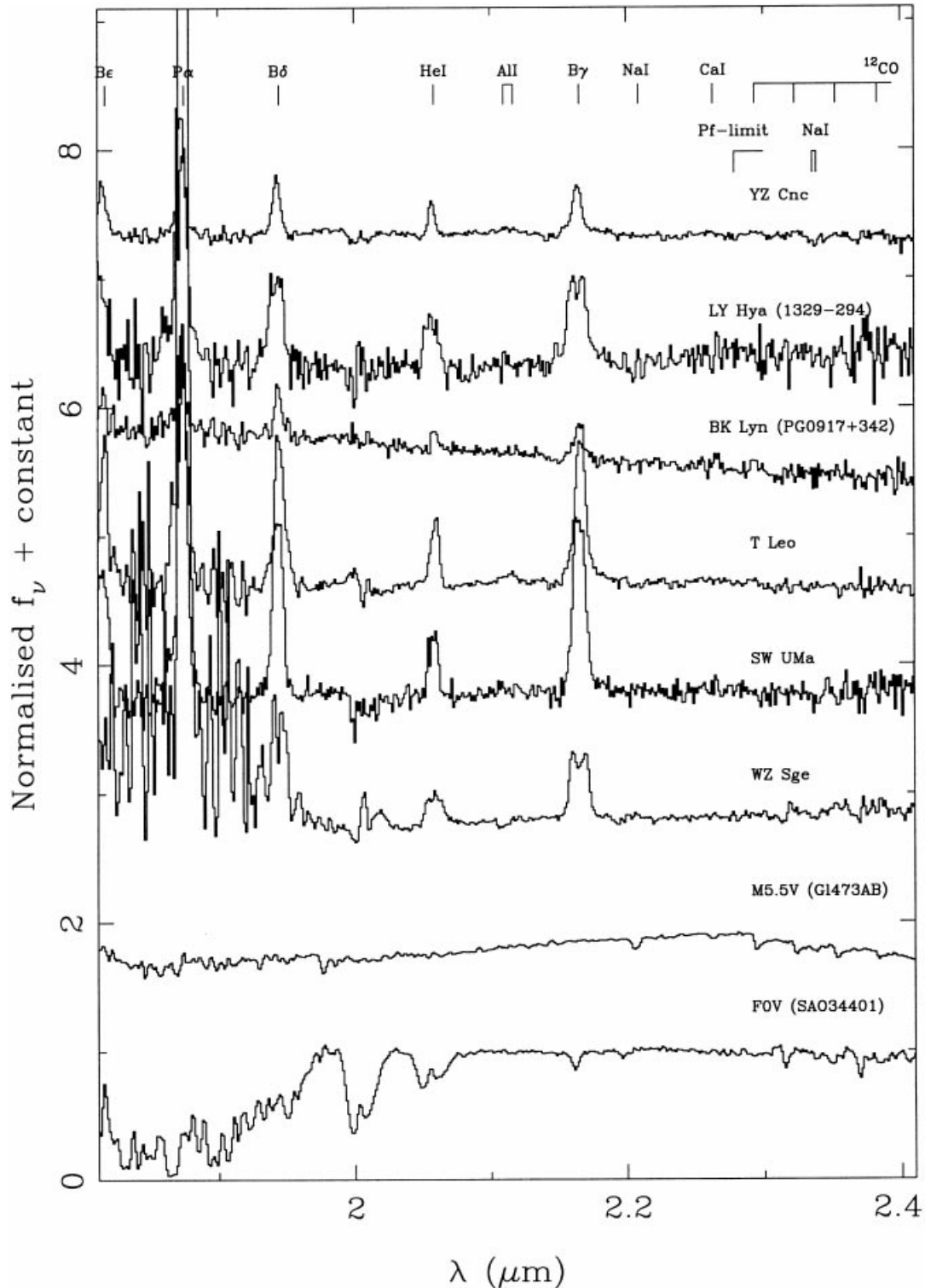© 2000 RAS, MNRAS **314**, 826–838

Figure 1. *K*-band spectra of the dwarf novae YZ Cnc, LY Hya, BK Lyn, T Leo, SW UMa, WZ Sge and an M5.5V star. The spectra have been normalized by dividing by the flux at 2.24 μm and then offset by adding a multiple of 0.9 to each spectrum. Also shown is the spectrum of an F0V star, normalized by dividing by a spline fit to its continuum, which indicates the location of telluric absorption features; spectral features within the strongest absorption bands are highly uncertain.

suffered from a little high cirrus. In order to compensate for fluctuating atmospheric OH^- emission lines (Ramsay, Mountain & Geballe 1992), we took relatively short exposures and nodded the telescope primary so that the object spectrum switched between two different spatial positions on the detector. A full journal of observations is presented in Table 1.

3 DATA REDUCTION

The initial steps in the reduction of the 2D frames were performed automatically by the CGS4 data reduction system (Daley & Beard 1994). These were the application of the bad pixel mask, bias and dark frame subtraction, flat-field division, interlacing integrations
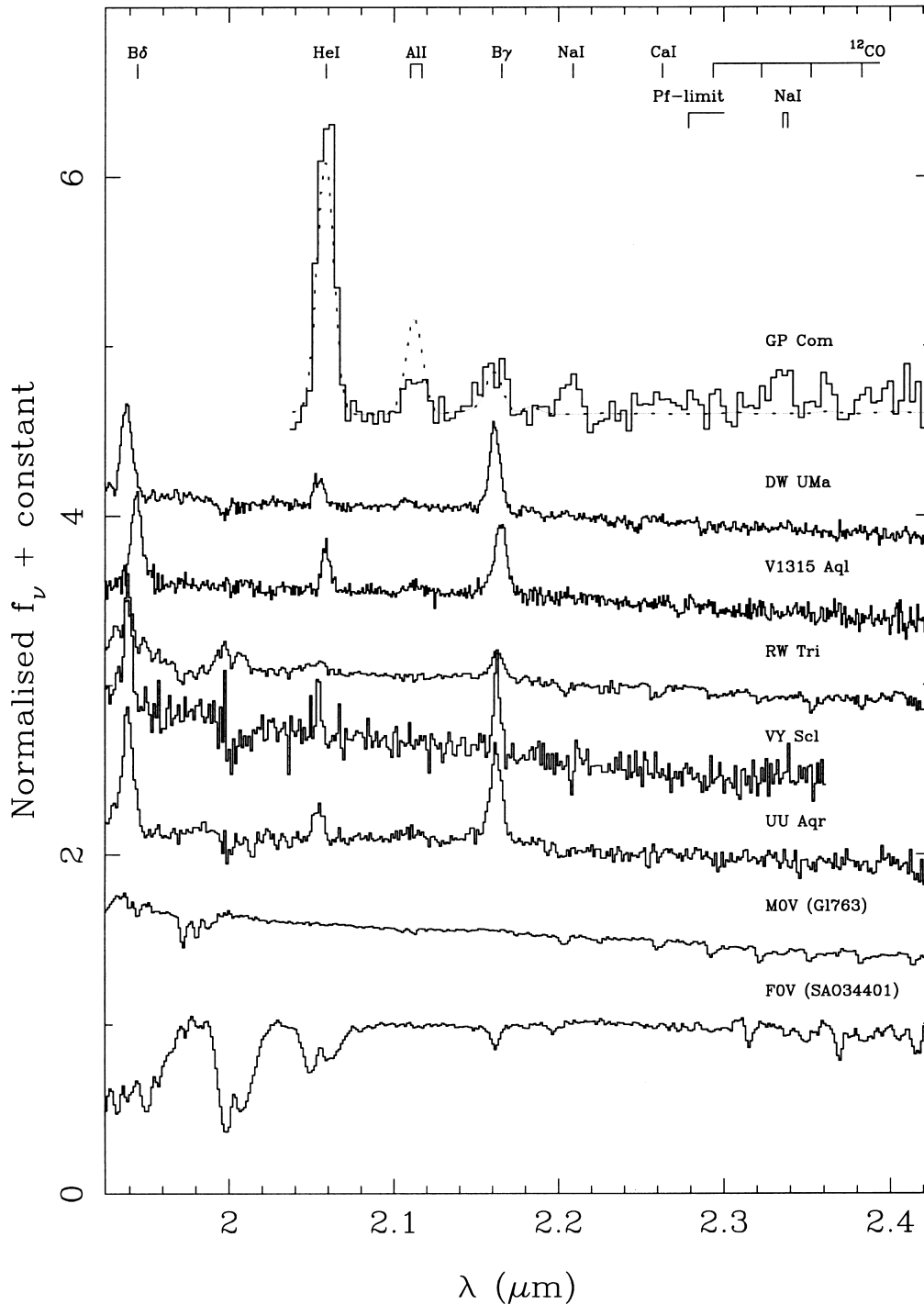
Figure 2. *K*-band spectra of the nova-like variables GP Com, DW UMa, V1315 Aql, RW Tri, VY Scl, UU Aqr and an M0V star. The spectra have been normalized by dividing by the flux at 2.24 μm and then offset by adding a multiple of 0.5 to each spectrum. Also shown is the spectrum of an F0V star, normalized by dividing by a spline fit to its continuum, which indicates the location of telluric absorption features; spectral features within the strongest absorption bands are highly uncertain. The dashed line under the spectrum of GP Com is a model spectrum from gas in LTE (see Section 4.1 for details).

taken at different detector positions, and coadding and subtracting nodded frames. Further details of the above procedures may be found in the review by Joyce (1992). In order to obtain 1D data, we subtracted the residual sky and then optimally extracted the spectra (Horne 1986).

There were three stages to the calibration of the spectra. The first was the calibration of the wavelength scale using argon arc-lamp exposures. The second-order polynomial fits to the arc lines always

yielded an error of less than 0.0003 μm (rms). The next step was the removal of the ripple arising from variations in the star brightness between integrations (i.e. at different detector positions). These variations were caused by changes in the seeing, sky transparency and the slight motion of the stellar image relative to the slit. We discovered that the amplitude of the ripple varied across the spectrum and we were thus forced to apply a correction for this based on a linear interpolation of the ripple profiles at either end of
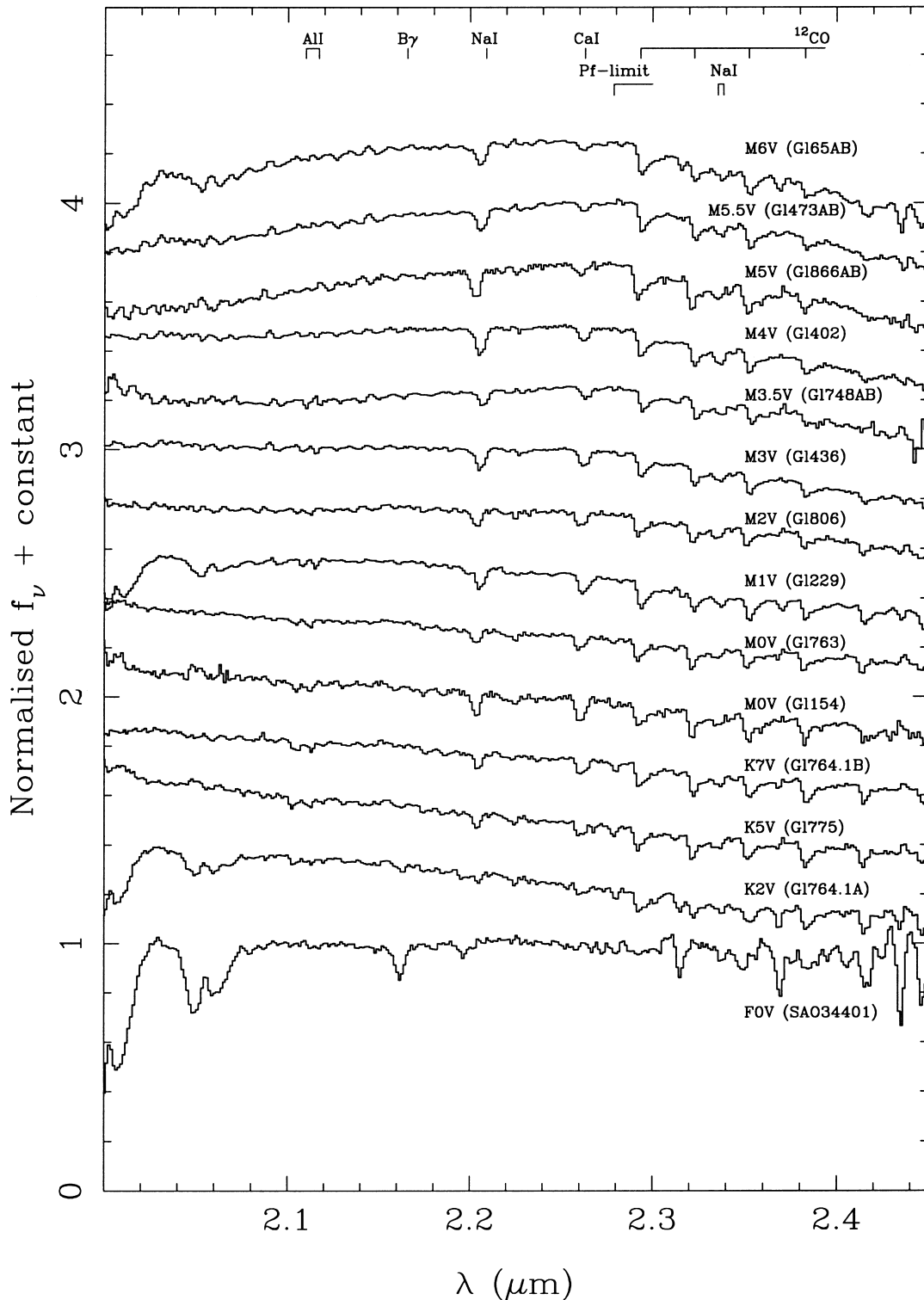
Figure 3. *K*-band spectra of K2V–M6V spectral-type template stars. The spectra have been normalized by dividing by the flux at 2.24 μm and then offset by adding a multiple of 0.25 to each spectrum. Also shown is the spectrum of an F0V star, normalized by dividing by a spline fit to its continuum, which indicates the location of telluric absorption features; spectral features within the strongest absorption bands are highly uncertain.

the spectrum. The final step in the spectral calibration was the removal of telluric atmospheric features and flux calibration. This was performed by dividing the spectra to be calibrated by the spectrum of an F-type standard, observed at a similar airmass (typically within 0.1), with its prominent stellar features masked

out. We then multiplied the result by the known flux of the standard at each wavelength, determined using a blackbody function set to the same temperature and magnitude as the standard. As well as providing flux-calibrated spectra, this procedure also removed atmospheric absorption features from the object spectra.

Table 2. Wavelengths, equivalent widths and velocity widths of the most prominent lines visible in the IR spectra of the surveyed CVs. The line identifications have been based upon the list presented by Dhillon & Marsh (1995) and references therein. The wavelengths given for the ^{12}CO lines refer to the band-heads. The vertical bars following lines of similar wavelength indicate that the equivalent width measurements apply to the entire blend. The two-letter codes indicate that a line was either not present (np) or present but not measurable (nm).

Line	λ (μm)	VY Scl EW (Å)	FWHM (km s⁻¹)	FWZI (km s⁻¹)	RW Tri EW (Å)	FWHM (km s⁻¹)	FWZI (km s⁻¹)	UU Aqr EW (Å)	FWHM (km s⁻¹)	FWZI (km s⁻¹)	LY Hya EW (Å)	FWHM (km s⁻¹)	FWZI (km s⁻¹)	YZ Cnc EW (Å)	FWHM (km s⁻¹)	FWZI (km s⁻¹)
B-ϵ	1.8174	nm	nm	nm	nm	nm	nm	nm	nm	nm	nm	3000 ± 1000	nm	nm	1050 ± 100	nm
P-α	1.8751	nm	nm	nm	nm	nm	nm	nm	nm	nm	170 ± 20	2200 ± 150	5200 ± 400	37 ± 4	900 ± 100	2200 ± 200
B-δ	1.9446	42 ± 5	800 ± 80	2600 ± 400	nm	nm	nm	42 ± 5	940 ± 90	3200 ± 400	94 ± 8	1800 ± 100	5900 ± 500	22 ± 2	960 ± 90	2500 ± 200
He I	2.0587	6 ± 2	380 ± 50	1100 ± 200	4 ± 1	750 ± 200	1300 ± 400	7 ± 2	730 ± 70	1300 ± 400	34 ± 5	1400 ± 100	2900 ± 400	9 ± 1	710 ± 70	2200 ± 200
B-γ	2.1655	27 ± 4	730 ± 70	1500 ± 200	16 ± 1	1100 ± 300	2000 ± 400	56 ± 2	930 ± 90	2800 ± 200	103 ± 6	2200 ± 100	3900 ± 200	36 ± 1	1200 ± 100	3000 ± 400
Al I	2.1099	np	np	np	nm	nm	nm	np	np	np	np	np	np	np	np	np
Al I	2.1170	np	np	np	nm	nm	nm	np	np	np	np	np	np	np	np	np
Na I	2.2062	np	np	np	−2.8 ± 0.5	nm	nm	np	np	np	np	np	np	np	np	np
Na I	2.2090															
Ca I	2.2614															
Ca I	2.2631	np	np	np	−1.9 ± 0.9	nm	nm	np	np	np	np	np	np	np	np	np
Ca I	2.2657															
^{12}CO	2.2935	np	np	np	−2 ± 1	nm	nm	np	np	np	np	np	np	np	np	np
^{12}CO	2.3227	np	np	np	−5 ± 1	nm	nm	np	np	np	np	np	np	np	np	np
Na I	2.3355															
Na I	2.3386															
^{12}CO	2.3525	np	np	np	−7 ± 1	nm	nm	np	np	np	np	np	np	np	np	np
^{12}CO	2.3830	np	np	np	−2 ± 1	nm	nm	np	np	np	np	np	np	np	np	np

Line	λ	SW UMa EW	FWHM	FWZI	T Leo EW	FWHM	FWZI	BK Lyn EW	FWHM	FWZI	WZ Sge EW	FWHM	FWZI
B-ϵ	1.8174	nm	1600 ± 200	nm	nm	1200 ± 200	nm	nm	600 ± 200	nm	nm	nm	nm
P-α	1.8751	244 ± 9	1300 ± 100	4500 ± 200	157 ± 6	1600 ± 100	3700 ± 200	30 ± 5	800 ± 80	1900 ± 200	nm	nm	nm
B-δ	1.9446	128 ± 5	1300 ± 100	2300 ± 200	93 ± 3	1300 ± 100	4000 ± 200	18 ± 3	850 ± 80	1800 ± 200	nm	nm	nm
He I	2.0587	34 ± 3	920 ± 90	2000 ± 200	32 ± 2	980 ± 90	2300 ± 200	5 ± 2	580 ± 50	2200 ± 400	26 ± 1	1600 ± 100	3800 ± 200
B-γ	2.1655	147 ± 4	1400 ± 100	3500 ± 200	119 ± 2	1400 ± 100	3500 ± 200	21 ± 2	920 ± 150	2900 ± 200	80 ± 1	2200 ± 150	3400 ± 200
Al I	2.1099	np	np	np	np	np	np	np	np	np	nm	nm	nm
Al I	2.1170	np	np	np	np	np	np	np	np	np	nm	nm	nm
Na I	2.2062	np	np	np	np	np	np	np	np	np	nm	nm	nm
Na I	2.2090												
Ca I	2.2614												
Ca I	2.2631	np	np	np	np	np	np	np	np	np	nm	nm	nm
Ca I	2.2657												
^{12}CO	2.2935	np	np	np	np	np	np	np	np	np	nm	nm	nm
^{12}CO	2.3227	np	np	np	np	np	np	np	np	np	nm	nm	nm
Na I	2.3355												
Na I	2.3386												
^{12}CO	2.3525	np	np	np	np	np	np	np	np	np	nm	nm	nm
^{12}CO	2.3830	np	np	np	np	np	np	np	np	np	nm	nm	nm

Table 2 – *continued*

Line	λ (µm)	DW UMa EW (Å)	FWHM (km s^{-1})	FWZI (km s^{-1})	V1315 Aql EW (Å)	FWHM (km s^{-1})	FWZI (km s^{-1})	GP Com EW (Å)	FWHM (km s^{-1})	FWZI (km s^{-1})
B-ϵ	1.8174	nm	nm	nm	nm	nm	nm	nm	nm	nm
P-α	1.8751	79 ± 3	850 ± 30	1900 ± 160	61 ± 8	1200 ± 100	3400 ± 200	nm	nm	nm
B-δ	1.9446	31 ± 1	930 ± 150	2200 ± 200	32 ± 2	1100 ± 100	2200 ± 200	nm	nm	nm
He I	2.0587	7 ± 1	730 ± 50	1800 ± 200	11 ± 1	820 ± 80	1600 ± 200	200 ± 7	1660 ± 70	4100 ± 150
B-γ	2.1655	44 ± 1	1130 ± 20	3200 ± 150	46 ± 1	1400 ± 50	2600 ± 200	51 ± 7	2600 ± 400	4400 ± 400
Al I	2.1099	np	np	np	np	np	np	np	np	np
Al I	2.1170	np	np	np	np	np	np	np	np	np
Na I	2.2062	np	np	np	np	np	np	np	np	np
Na I	2.2090									
Ca I	2.2614									
Ca I	2.2631	np	np	np	np	np	np	np	np	np
Ca I	2.2657									
^{12}CO	2.2935	np	np	np	np	np	np	np	np	np
^{12}CO	2.3227									
Na I	2.3355	np	np	np	np	np	np	np	np	np
Na I	2.3386									
^{12}CO	2.3525	np	np	np	np	np	np	np	np	np
^{12}CO	2.3830	np	np	np	np	np	np	np	np	np

Table 3. Wavelengths and equivalent widths (in Å) of the most prominent lines visible in the IR spectra of the surveyed dwarf stars. The line identifications have been based upon the list presented by Dhillon & Marsh (1995) and references therein. The wavelengths given for the ^{12}CO lines refer to the band-heads. Equivalent widths for the H$_2$0 band were measured between 2.29 and 2.44 μm. The vertical bars following lines of similar wavelength indicate that the equivalent width measurements apply to the entire blend. The two-letter codes indicate that a line was either not present (np) or present but not measurable (nm). Note that the values indicated by asterisks are subject to unknown systematic errors caused by difficulties in continuum normalization.

Line	λ (μm)	Gl764.1A K2V	Gl775 K5V	Gl764.1B K7V	Gl154 M0V	Gl763 M0V	Gl229 M1V	Gl806 M2V	Gl436 M3V	Gl748AB M3.5V	Gl402 M4V	Gl866AB M5V	Gl473AB M5.5V	Gl65AB M6V
Al I	2.1099	nm	−4.3 ± 0.5	−3.7 ± 0.6	−3.1 ± 0.6	−2.1 ± 0.4	−1.3 ± 0.3	−1.3 ± 0.4	−0.8 ± 0.4	nm	nm	nm	nm	nm
Al I	2.1170													
Na I	2.2062	nm	−2.1 ± 0.4	−2.9 ± 0.4	−3.2 ± 0.6	−3.0 ± 0.3	−4.2 ± 0.4	−3.8 ± 0.4	−4.9 ± 0.4	−3.1 ± 0.4	−6.7 ± 0.5	−6.6 ± 0.6	−5.8 ± 0.3	−6.5 ± 0.4
Na I	2.2090													
Ca I	2.2614													
Ca I	2.2631	−1.2 ± 0.4	−2.9 ± 0.4	−3.1 ± 0.5	−3.5 ± 0.5	−2.9 ± 0.5	−6.4 ± 0.4	−4.4 ± 0.4	−4.3 ± 0.4	−2.9 ± 0.4	−4.6 ± 0.5	−6.0 ± 0.7	−3.5 ± 0.3	−2.3 ± 0.3
Ca I	2.2657													
H$_2$0	2.2900	−26 ± 2	−35 ± 2	−80 ± 2	−61 ± 3	−62 ± 2	−72 ± 2*	−152 ± 2	−194 ± 1	−222 ± 2	−249 ± 2	−346 ± 2	−315 ± 1	−235 ± 2
^{12}CO	2.2935	−3.3 ± 0.6	−1.9 ± 0.6	−3.6 ± 0.6	−9 ± 1	−3.1 ± 0.7	−16 ± 1*	−3.9 ± 0.6	−2.0 ± 0.6	−3.8 ± 0.5	−4 ± 1	−6.1 ± 0.8	−4.0 ± 0.4	−3.9 ± 0.5
^{12}CO	2.3227													
Na I	2.3355	−4 ± 1	−5.1 ± 0.7	−6.5 ± 0.8	−14 ± 1	−4.8 ± 0.9	−20 ± 1*	−7.2 ± 0.8	−6.9 ± 0.7	−9.0 ± 0.7	−11 ± 1	−12 ± 1	−9.8 ± 0.6	−8.7 ± 0.6
Na I	2.3386													
^{12}CO	2.3525	−2.0 ± 0.8	−4.4 ± 0.8	−4.1 ± 0.9	−14 ± 1	−1.6 ± 0.9	−18 ± 1*	−3.1 ± 0.8	−4.7 ± 0.7	−5.2 ± 0.7	−5 ± 1	−7.5 ± 1	−6.1 ± 0.6	−5.5 ± 0.8
^{12}CO	2.3830	−0.5 ± 0.9	−2.4 ± 0.8	−2 ± 1	−11 ± 1	−1.5 ± 0.8	−11 ± 1*	−1.6 ± 0.7	−3.5 ± 0.7	−2.0 ± 0.8	−2 ± 1	−1.2 ± 0.9	−2.1 ± 0.5	−1.2 ± 0.6

4 RESULTS

Fig. 1 shows the *K*-band spectra of the dwarf novae YZ Cnc, LY Hya, BK Lyn, T Leo, SW UMa and WZ Sge, and Fig. 2 shows the *K*-band spectra of the nova-like variables GP Com, DW UMa, V1315 Aql, RW Tri, VY Scl and UU Aqr. Note that the anti-dwarf novae DW UMa and VY Scl were both in their high state when the spectra in Fig. 2 were obtained. In Fig. 3 we show the *K*-band spectra of main-sequence field dwarfs ranging in spectral type from K2 to M6 and in Tables 2 and 3 we list the wavelengths, equivalent widths and velocity widths of the most prominent spectral lines identified in Figs 1, 2 and 3.

4.1 Emission lines

The spectra of the dwarf novae below the period gap in Fig. 1 are dominated by strong emission lines of He I and the Paschen and Brackett series of H I. The large velocity and equivalent widths of these lines (see Table 2) indicate an accretion disc origin. This conclusion is further supported by the double-peaked emission-line profiles exhibited by the high-inclination dwarf novae LY Hya and WZ Sge (see also Skidmore et al. 2000 and Mason et al. 2000) in Fig. 1.

With the exception of the double-degenerate system GP Com, which will be discussed in more detail below, the spectra of the nova-like variables in Fig. 2 are dominated by strong, single-peaked emission lines of H I (Brackett γ and Brackett δ) and He I (2.0587 μm). This is in stark contrast to what one might expect from standard accretion disc theory (e.g. Horne & Marsh 1986), which predicts that emission lines from high-inclination discs, such as those in the eclipsing systems DW UMa, V1315 Aql, RW Tri and UU Aqr, should appear double-peaked. The absence of double-peaked profiles in high-inclination nova-likes is also observed in the optical (see Dhillon 1996) and is one of the defining characteristics of the so-called SW Sex stars, of which DW UMa, V1315 Aql and UU Aqr are members.

GP Com consists of a CO white dwarf and a helium degenerate star in an orbit of 46 min period. Neither star is directly visible – the optical light from the system is dominated by the accretion disc, which has a spectrum composed almost entirely of helium and nitrogen emission lines reflecting the products of hydrogen burning and CNO processing in the helium degenerate donor. A very simple model, based upon local thermodynamic equilibrium (LTE) emission from an ∼11 000 K optically thin (in the continuum) slab provides a surprisingly good fit to the optical spectrum of GP Com (Marsh, Horne & Rosen 1991). In Fig. 2, the same model has been applied to the IR spectrum of GP Com, with equally good results. The model predicts the existence of three strong emission lines in the *K* band, all of He I, which are all present in the actual spectrum. Note that there is also some evidence for a fourth emission line in the spectrum at 2.2 μm, apparently unrelated to any telluric features, which we have been unable to identify.

4.2 Absorption lines/bands

RW Tri is the only CV presented in Figs 1 and 2 that shows absorption features from the secondary star – one can clearly make out the profiles of Al I, Na I, Ca I and ^{12}CO in the spectrum. The distinctive water absorption band at ∼2.3 μm, so prominent in the spectra of the late M stars presented in Fig. 3, is absent in

RW Tri, indicating that its secondary is most likely a late K dwarf. In order to estimate the spectral type of the secondary star in RW Tri from our data, and to determine its contribution to the total *K*-band flux, we used an optimal subtraction technique (e.g. Dhillon & Marsh 1993). First, we normalized the spectra of RW Tri and the template stars by dividing by a third-order polynomial fit to the continuum. A constant times the normalized template spectrum was then subtracted from the normalized spectrum of RW Tri and the constant adjusted so as to minimize the residual scatter in regions containing secondary star features. The residual scatter is measured by carrying out the subtraction and then computing the χ^2-value between the residual spectrum and a smoothed version of itself. Prior to the subtraction, the template spectra should be broadened to account for the rotational velocity of the secondary star; the low resolution of our data, however, made this step unnecessary. The value obtained for the percentage contribution naturally depends on spectral type, the correct spectral type being the one that minimizes the value of χ^2. Using this method we find that the secondary star contributes 65 ± 5 per cent (1σ error) of the *K*-band light in RW Tri and that the spectral type of the secondary star is M0V. This spectral-type determination is in good agreement with the results of the skew mapping experiments of Smith, Cameron & Tucknott (1993), who derive a spectral type of K7V or cooler, and with the predictions of the main-sequence spectral type–period relationship of Smith & Dhillon (1998), which suggests a spectral type of K9V.

None of the other CVs shows any signs of absorption features from the secondary star. In these cases it is possible to determine an upper limit to the contribution of the secondary star. This is done by subtracting a constant times the normalized template spectrum from the normalized CV spectrum, until spectral absorption features from the template star appear in emission in the CV spectrum. The value of the constant at this point represents an upper limit to the fractional contribution of the secondary star. The contribution found depends on the spectral type of the template used. As the spectral type of the secondary star is unknown for these systems, we used the period–spectral type relationship of Smith & Dhillon (1998) to select an appropriate spectral type for the template star. The spectral type used for each CV, along with the corresponding upper limits to the secondary star contribution, is listed in Table 4.

It is seen that the secondary star contributes less than 30–55 per cent for the nova-likes and 10–30 per cent for the dwarf novae below the period gap. Exceptions are VY Scl and LY Hya, where poor signal-to-noise ratio has resulted in very high values – the significance of these results is that we would have to obtain better signal-to-noise ratio if we were to have any hope of observing the secondary in these systems, regardless of its contribution to the *K*-band light. A further exception is WZ Sge, in which the secondary must contribute less than 10 per cent of the *K*-band light. This is in agreement with Littlefair et al. (2000), who find that the secondary star in WZ Sge contributes less than 20 per cent to the *J*-band light, and Ciardi et al. (1998), who model the near-IR flux in WZ Sge and find that the secondary is a cool (∼1700 K) star, which contributes approximately 10 per cent of the overall IR flux.

4.3 Distances

The distances to CVs can be measured from *K*-band spectra using a modification of a method first proposed by Bailey (1981). The distance modulus can be rewritten in terms of the *K*-band surface

Table 4. Upper limits to the contributions of the secondary star to the total K-band flux.

Object	Secondary star contribution	Error	Spectral-type template used
VY Scl	90 per cent	10 per cent	M4V
DW UMa	35 per cent	5 per cent	M4V
V1315 Aql	30 per cent	5 per cent	M4V
UU Aqr	55 per cent	5 per cent	M4V
BK Lyn	50 per cent	5 per cent	M5V
LY Hya	100 per cent	10 per cent	M5V
YZ Cnc	20 per cent	5 per cent	M5V
SW UMa	20 per cent	5 per cent	M5.5V
T Leo	30 per cent	5 per cent	M5.5V
WZ Sge	10 per cent	5 per cent	M5.5V

brightness as

$$S_k = m_K + 5 - 5 \log d + 5 \log(R/R_\odot), \tag{1}$$

where m_K is the apparent K-band magnitude, d is the distance in pc and R is the radius of the star. For a star of one solar radius, S_k is equal to the absolute K-band magnitude. Since the radius of the secondary star is equal to the radius of the Roche lobe, the orbital period and mass of the secondary are sufficient to determine its radius (there is also a weak dependance on mass ratio). m_K is derived from the K-band magnitude of the CV and the percentage contribution of the secondary star. Given m_K and the value of S_k, which can be obtained from the $V - K$ colour (or spectral type) of the secondary using the empirical calibrations derived from field dwarfs by Ramseyer (1994), it is possible to estimate the distance using the above equation. Note that the distances to only 5 of the surveyed CVs are estimated here, as the remaining 7 CVs do not have published K-band magnitudes.

4.3.1 RW Tri

The K-band magnitude of RW Tri is 11.59 (Longmore et al. 1981). In conjunction with the percentage contribution estimated in Section 4.2, this gives a K-band magnitude for the secondary star of $m_K = 12.06 \pm 0.08$. Assuming the error in S_k is dominated by the error in spectral type (estimated to be one spectral type sub-classification), Bessell (1991) gives a $V - K$ colour for the secondary of $V - K = 3.65 \pm 0.1$. Using the calibrations in (Ramseyer 1994), this gives $S_k = 4.43 \pm 0.1$. We have estimated the radius of the secondary to be $R/R_\odot = (0.61 \pm 0.2)$ from the orbital period–radius relation (equation 11) given by Smith & Dhillon (1998). These values, in conjunction with equation 1 give a distance to RW Tri of $d = 205 \pm 90$ pc. McArthur et al. (1999) used the *Hubble Space Telescope* (*HST*) to obtain a parallax for RW Tri, establishing the distance to RW Tri at 341^{-31}_{+38} pc. The discrepancy in the two results may be caused by the fact that the actual K-band magnitude of RW Tri at the time of our observation is unknown and we have had to adopt the value obtained by (Longmore et al. 1981). We know, however, that there is a long-term variation in the V-band magnitude of RW Tri at primary minimum, ranging from 13.7 to 15.4, suggesting that there is an uneclipsed, variable component (Longmore et al. 1981). One might expect to see variation on a similar scale in the K band (the actual long-term K-band variation has never been recorded), in which case our results are consistent with distances ranging from 90–400 pc.

4.3.2 WZ Sge

The K magnitude of WZ Sge is 13.3 (Ciardi et al. 1998), which in conjunction with our upper limit to the secondary star contribution implies that $m_K \geqslant 15.8$. Smak (1993) estimates the radius of the secondary to be $R_2/R_\odot = 0.11$. Determining S_k is more problematic. Ciardi et al. (1998) find evidence that the secondary in WZ Sge is very cool (less than 1700 K), and Littlefair et al. (2000) use distance estimates by Spruit & Rutten (1998) and Smak (1993) to constrain the spectral type of the secondary to be later than M7.5. S_k for M7.5 (from Bessell 1991) is 6.8 and we shall adopt this value. Using these values we obtain a distance to WZ Sge of $d \geqslant 69$ pc. Spruit & Rutten (1998) and Smak (1993) both found a distance to WZ Sge of 48 pc by fitting white dwarf models to UV spectra of WZ Sge obtained using the *HST* and the *International Ultraviolet Explorer* (*IUE*), respectively.

4.3.3 T Leo

The K magnitude of T Leo is 14.01 (Sproats, Howell & Mason 1996), which implies $m_K \geqslant 15.3$. We have estimated the radius of the secondary from the orbital period–radius relation given by Smith & Dhillon (1998). Likewise, S_k follows from the data in Bessell (1991) and a spectral type estimated from the orbital period–spectral type relationship in Smith & Dhillon (1998). Using these values we find $d \geqslant 120$ pc, close to the value of $d \sim 100$ pc found by Howell et al. (1999).

4.3.4 YZ Cnc

The K magnitude of YZ Cnc is 14.37 (Sherrington & Jameson 1983), which implies $m_K \geqslant 16$. Again, we estimate S_k and the radius of the secondary star from the orbital period and the relationships given by Smith & Dhillon (1998). We find $d \geqslant 290$ pc. Patterson (1984) finds a distance to YZ Cnc of ~ 130 pc, using a method based on the equivalent width of Hβ and the shape of the continuum. The large discrepancy between these numbers is almost certainly the result of the relatively unreliable techniques that Patterson (1984) was forced to use.

4.3.5 BK Lyn

The K magnitude of BK Lyn is 14.63 (Sproats et al. 1996). Following the same method as for YZ Cnc and T Leo, we obtain $d \geqslant 185$ pc. Note that Dobrzycka & Howell (1992) derived a value of $d \sim 1000$ pc, but this was based upon the assumption that the absolute magnitude of BK Lyn is the same as that typically found for nova-likes (i.e. $M_V \sim +4$), and is hence highly uncertain.

4.4 Time-resolved spectra

Time-resolved spectra were obtained for T Leo, SW UMa, YZ Cnc and WZ Sge. Unfortunately, a combination of poor signal-to-noise ratio and velocity resolution means that radial velocity studies and Doppler tomography were fruitless (with the exception of WZ Sge – see Skidmore et al. 2000 and Mason et al. 2000). Skew mapping (see Smith et al. 1993) was performed, but no systems showed signs of the secondary star. Equivalent width light curves were obtained for all stars, but only those of T Leo and YZ Cnc show significant features, and are described here.
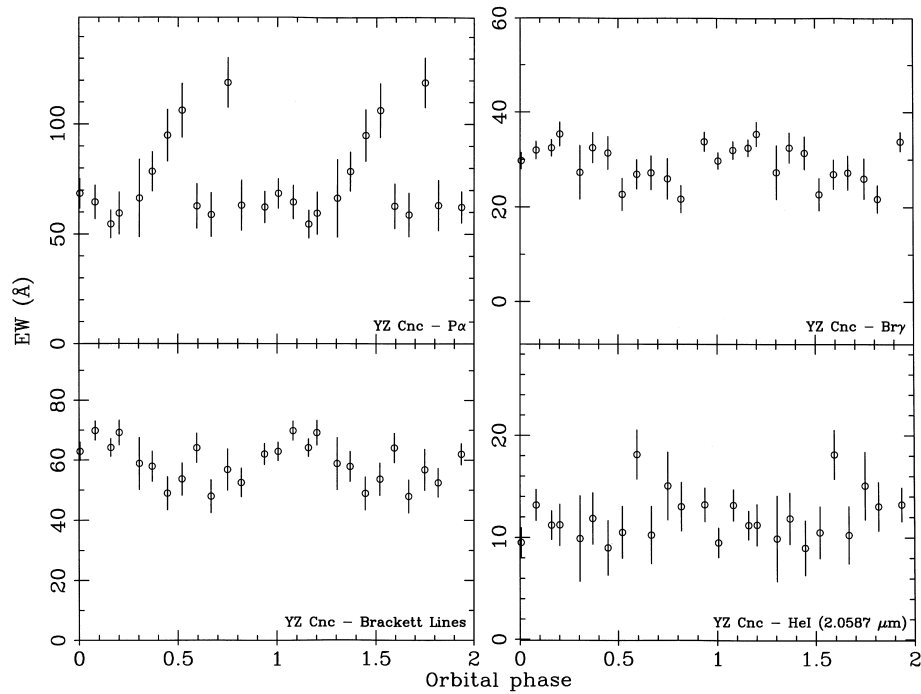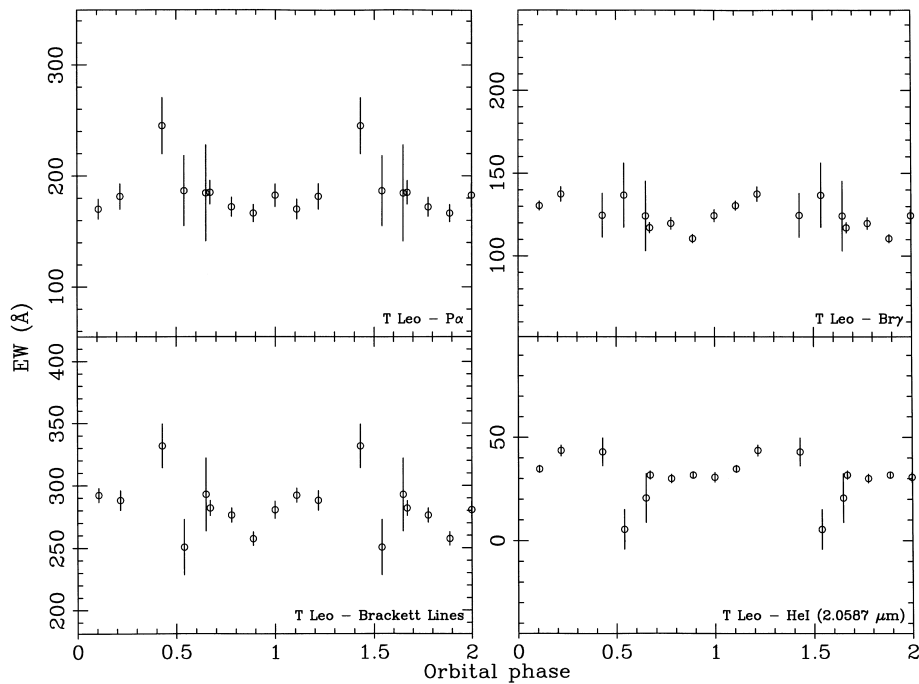
Figure 4. Equivalent width (EW) light curves of YZ Cnc. The light curves have been folded over two orbital cycles for clarity, according to the ephemeris of van Paradijs et al. (1994). Paschen α was determined in the range 1.854–1.890 μm, Brackett γ in the range 2.153–2.173 μm, He I in the range 2.053–2.062 μm and the sum of the Brackett γ and Brackett δ lines in the ranges 1.933–1.952 and 2.153–2.173 μm.

Figure 5. Equivalent width (EW) light curves of T Leo. The light curves have been folded over two orbital cycles for clarity, according to the ephemeris of Shafter & Szkody (1984). Paschen α was determined in the range 1.854–1.890 μm, Brackett γ in the range 2.153–2.173 μm, He I in the range 2.053–2.062 μm and the sum of the Brackett γ and Brackett δ lines in the ranges 1.933–1.952 and 2.153–2.173 μm.

4.4.1   YZ Cnc

Fig. 4 shows the equivalent width light curves for YZ Cnc. Both the Brackett lines and He I show a modulation on the orbital period, with maximum light at $\phi \sim 0.0$. van Paradijs et al. (1994)

find a similar modulation in the optical data, but with different phasing, with maximum light at $\phi \sim 0.8$. They attribute this to bright spot modulations. It is likely that the modulations we observe in the K band share the same source, given that the discrepancy in phase is well within the error quoted for the

ephemeris given by van Paradijs et al. (1994). The variation is not as marked in the *K* band as in the optical, perhaps suggesting that the bright spot contributes relatively less light to the system in the IR.

The Paschen α line in YZ Cnc shows unusual behaviour, but this line is strongly affected by telluric features and hence the data are uncertain.

4.4.2 T Leo

Fig. 5 shows the equivalent width light curves for T Leo. The data are of poorer time resolution and signal-to-noise ratio than the YZ Cnc data of Fig. 4. Paschen α and the Brackett lines appear to show a similar variation to that observed in YZ Cnc, with the exception that maximum light is now located at $\phi \sim 0.4$. Phase should not be taken as reliable in this case, as a considerable time has elapsed since the ephemeris of Shafter & Szkody (1984) was determined. We suggest that this variation may possibly be caused by bright spot modulations, as in YZ Cnc, but poor signal-to-noise ratio and errors in phasing make this conclusion uncertain. The He I line does not show clear modulations with orbital phase.

5 DISCUSSION

The prospects of studying the secondary stars in nova-like variables (particularly the SW Sex type systems just above the period gap) and dwarf novae below the period gap appears bleak. With a few rare exceptions, the secondary star cannot even be detected, let alone studied. This, in turn, means that an essential tool in the study of the evolution of these systems – a knowledge of the mass and spectral type of the secondary star – is currently unavailable.

Why are the secondary stars so difficult to detect in these systems? In the case of the dwarf novae below the period gap, this is almost certainly due to the low surface temperature and small size of the secondary star, with the secondary contributing no more than $10-30$ per cent of the total *K*-band light. This compares with the easily detectable secondary stars in dwarf novae above the period gap, which typically contribute at least 75 per cent of the *K*-band light (Dhillon & Marsh 1995).

Nova-like variables also lie above the period gap, however, so why are their secondary stars not visible? One explanation is that the steady-state accretion discs in nova-like variables are much brighter than the quiescent discs in dwarf novae of a similar orbital period; the resulting increase in shot noise from the disc spectrum overwhelms the weak signal from the secondary star. This does not explain, however, why the secondary star in DW UMa was not even visible during a $3-4$ mag low state (when accretion had virtually ceased) in the *I*-band spectra of Marsh & Dhillon (1997). This observation implies that the secondary star in DW UMa has an apparent magnitude of $I > 19.5$ and hence a distance of at least ~ 850 pc if the secondary star has spectral type M4. If this lower limit to the distance is typical of most nova-likes (or, specifically, SW Sex stars), then it means that the mass transfer rates derived from techniques such as eclipse mapping (e.g. Rutten, van Paradijs & Tinbergen 1992) are underestimating the true values.

ACKNOWLEDGMENTS

REFERENCES

Bailey J. A., 1981, MNRAS, 197, 31
Bessell M. S., 1991, AJ, 101, 662
Ciardi D. R., Howell S. B., Hauschildt P. H., Allard F., 1998, ApJ, 504, 450
Daley P. N., Beard S. M., 1994, Starlink User Note 27, Rutherford Appleton Laboratory
Dhillon V. S., 1996, in Evans A., Wood J. H., eds, Cataclysmic Variables and Related Objects. Kluwer Academic Publishers, Dordrecht, p. 3
Dhillon V. S., 1998, in Howell S. B., Kuulkers E., Woodwar C., eds, Wild Stars in the Old West: Proc. 13th North American Workshop on Cataclysmic Variables and Related Objects, ASP Conf. Ser. Vol. 137. Astron. Soc. Pac., San Francisco, p. 23
Dhillon V. S., Marsh T. R., 1993, in Regev O., Shaviv G., eds, Cataclysmic Variables and Related Physics. Inst. Phys. Publ., Bristol, p. 34
Dhillon V. S., Marsh T. R., 1995, MNRAS, 275, 89
Dhillon V. S., Marsh T. R., Duck S. R., Rosen S. R., 1997, MNRAS, 285, 95
Dobrzycka D., Howell S. B., 1992, ApJ, 388, 614
Friend M. T., Martin J. S., Smith R. C., Jones D. H. P., 1988, MNRAS, 233, 451
Gliese W., 1969, Vëroff. Astr. Rechen-Inst. Heidelberg, 22
Hawley S. L., Gizis J. E., Reid I. N., 1996, AJ, 112, 2799
Henry T. J., Kirkpatrick J. D., Simons D. A., 1994, AJ, 108, 1437
Horne K., 1986, PASP, 98, 609
Horne K., Marsh T. R., 1986, MNRAS, 218, 761
Howell S. B., Ciardi D. R., Szkody P., van Paradijs J., Kuulkers E., Cash J., Sirk M., Long K. S., 1999, PASP, 111, 342
Joyce R. R., 1992, in Howell S. B., ed., Astronomical CCD Observing and Reduction Techniques, ASP Conf. Ser. Vol. 23. Astron. Soc. Pac., San Francisco, p. 258
Kirkpatrick J. D., Henry T. J., McCarthy D. W. J., 1991, ApJS, 77, 417
Littlefair S. P., Dhillon V. S., Howell S. B., Ciardi D. R., 2000, MNRAS, 313, 117
Longmore A. J., Lee T. J., Allen D. A., Adams D. J., 1981, MNRAS, 195, 825
McArthur B. E. et al., 1999, ApJ, 520, 59
Marsh T. R., Dhillon V. S., 1997, MNRAS, 292, 385
Marsh T. R., Horne K., Rosen S. R., 1991, ApJ, 366, 535
Mason E., Skidmore W., Howell S. B., Ciardi D. R., Littlefair S. P., Dhillon V. S., 2000, MNRAS, submitted
Patterson J., 1984, ApJS, 54, 443
Ramsay S. K., Mountain C. M., Geballe T. R., 1992, MNRAS, 259, 751
Ramseyer T. F., 1994, ApJ, 425, 243
Ringwald F. A., Thorstensen J. R., Honeycutt R. K., Robertson J. W., 1996, MNRAS, 278, 125
Ritter H., Kolb U., 1998, A&AS, 129, 83
Rutten R. G. M., van Paradijs J., Tinbergen J., 1992, A&A, 260, 213
Shafter A. W., Szkody P., 1984, ApJ, 276, 305
Sherrington M. R., Jameson R. F., 1983, MNRAS, 205, 265
Skidmore W., Mason E., Howell S. B., Ciardi D. R., Littlefair S. P., Dhillon V. S., 2000, MNRAS, submitted
Smak J., 1993, Acta Astron., 43, 101
Smith D. A., Dhillon V. S., 1998, MNRAS, 301, 767
Smith R. C., Cameron A., Tucknott D. S., 1993, in Regev O., Shaviv G.,

eds, Cataclysmic Variables and Related Physics. Inst. Phys. Publ., Bristol, p. 70

Smith R. C., Sarna M. J., Catalan M. S., Jones D. H. P., 1997, MNRAS, 287, 271

Sproats L. N., Howell S. B., Mason K. O., 1996, MNRAS, 282, 1211

Spruit H. C., Rutten R. G. M., 1998, MNRAS, 299, 768

van Paradijs J. et al., 1994, MNRAS, 267, 465

Warner B., 1995, Cataclysmic Variable Stars. Cambridge Univ. Press, Cambridge

This paper has been typeset from a TEX/LATEX file prepared by the author.